Chapter 1
Surface Studies by Low-Energy Electron Diffraction and Reflection High-Energy-Electron Diffraction

P. Laukkanen, J. Sadowski, and M. Guina

Abstract In this chapter, we present the basic concepts of the low-energy electron diffraction (LEED) and reflection high-energy electron diffraction (RHEED) experiments. The main goal is to provide an overview of the exploitation of these instrumental methods for analyzing the surfaces of technologically important III–V compound semiconductors. In particular, the interpretation of LEED and RHEED patterns is discussed for the most representative reconstructions of GaAs(100), GaInAsN(100), and Bi-stabilized III–V(100) surfaces. Other application examples concern the use of RHEED for optimizing the growth conditions and growth rates used in molecular beam epitaxy of III–V device heterostructures.

1.1 Basics of RHEED and LEED

The ability to synthesize novel semiconductor compounds and to study their crystalline properties and interfaces is essential for the development of new electronic and optoelectronic devices. Nobel laureate Herbert Kroemer has described the importance of device interfaces as follows: "Often, it may be said that the interface is the device" [1]. However, the controlled fabrication of high-quality interfaces is not straightforward because the surface of a crystal forming the interface is usually the most defective part of the material. In addition, the atomic structures of semiconductor surfaces often differ from the structures of the corresponding planes deeper in the crystal (bulk) because on many semiconductor surfaces, the bulk-plane structure is not energetically favored. This indeed affects the properties of the semiconductor surfaces and the interface formation. In general, any improvement in

P. Laukkanen (✉)
Department of Physics and Astronomy, University of Turku, FI-20014 Turku, Finland
Optoelectronics Research Centre, Tampere University of Technology, FI-33101 Tampere, Finland
e-mail: peklau@utu.fi

the crystal ordering at the interface or in the film will decrease the density of harmful interface defects. Crystalline interfaces and thin films are also essential for investigating the fundamental properties of these materials because the interpretation of measured data from an amorphous (not well-defined) material is often challenging. The diffraction-based analysis techniques are very useful for understanding and engineering the properties of crystalline layers and junctions. This chapter deals with the characterization of several technologically relevant semiconductor surface layers by means of two surface-sensitive measurements: reflection high-energy electron diffraction (RHEED) and low-energy electron diffraction (LEED), which visualize the reciprocal lattice of a surface layer studied. RHEED is the standard equipment in the epitaxial growth chambers providing a great opportunity to monitor surface properties during the growth process. This real-time in-situ method makes it possible to control the growth with atomic layer precision. In contrast, the LEED characterization is usually done in a separate vacuum chamber that is connected to an epitaxial growth chamber. LEED measurements are particularly useful in determining the surface geometry of the starting substrate used for interface growth, such as an insulator–semiconductor interface. Both RHEED and LEED analyses are also excellent methods to solve detailed surface atomic structures via the comparison of angle or electron-energy dependent diffraction intensity with the corresponding intensity curves calculated and refined with the potential atomic models. While discussing several examples of LEED and RHEED patterns, our goal is to provide the reader with the basic tools to interpret own RHEED and LEED data. For an in-depth study of the instrumental and physical concepts, we recommend several excellent books and review articles, for example [2–10] given here.

Generally speaking, the instrumental part of LEED and RHEED consists of an electron gun and a luminescence screen that detects the electrons diffracted by the sample under study. Since its discovery in 1927 by Davisson and Germer [11, 12], LEED has become a widely used method for analyzing surface structures. In a typical LEED setup, the electrons are accelerated with voltage V of 10–500 V. Then the de Broglie wavelength of the electrons, $\lambda_E = h/(2m_E V e)^{1/2}$, ranges from 0.87 to 2.75 Å; these values are small enough for electrons to experience diffraction from semiconductor crystals. Here h is the Planck constant, m_E is electron rest mass, and e is the elementary charge. The LEED electron beam impinges on the surface along the surface-normal direction, and the elastically backscattered electrons give an intensity pattern which visualizes (or maps) the reciprocal lattice of the surface layer. On the basis of this information about the reciprocal lattice, the real-space surface lattice can be constructed. The mathematical relation between the lattice and reciprocal-lattice vectors can be found for example in [2–5]. The diffraction is described by the Laue condition: $k_{\parallel} = G$. Here G is the surface reciprocal lattice vector, and $k_{\parallel}$ is the parallel component of the change $(K_f - K_i)$ in which K_i and K_f are the incident and scattered wave vectors of the electron, as represented schematically in Fig. 1.1. The Laue equation also provides a physical meaning for the reciprocal vectors: every diffraction beam corresponds to the reciprocal vector. Because LEED operates in a low-energy regime, which is close to the minimum of
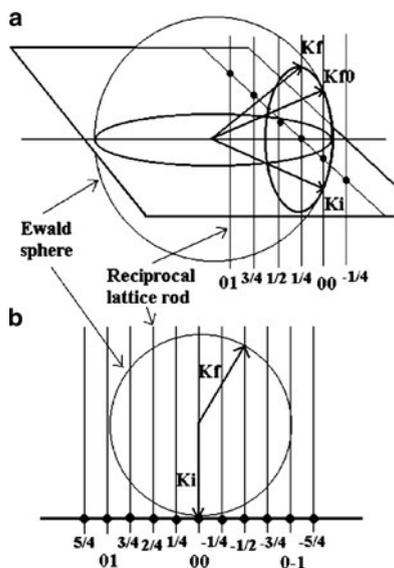
Fig. 1.1 The reciprocal Ewald-sphere constructions in (**a**) RHEED and (**b**) LEED for the ideal single plane of atoms, where the plane distance is infinite in the surface-normal direction in real space, corresponding to the infinitely small distance in reciprocal space; in other words, the reciprocal rods are formed along the surface normal. These rods intersect at the reciprocal lattice points (*black spots* in the plane) determined by the surface reciprocal vector G. The fractional order spots are due to a surface reconstruction. K_i and K_f are the incident and diffracted wave vectors of electrons; K_f^0 represents the specular reflection. The magnitude of the K vector is $2\pi/\lambda_E$ for the incident and elastically diffracted electrons. The intersections of the sphere and rods provide the diffraction directions. Data adapted from [2, 6]

the "universal" curve of electrons mean-free path in solids, the elastic scattering occurs mainly on the topmost layers. However, we should note that a LEED diffraction pattern would also include some signal from the bulk planes beneath the surface, i.e., the intensity for the (1×1) reference spots.

In RHEED, electrons are accelerated at much higher voltages (i.e., from about 5 to 50 kV). For a voltage of 10 kV, the de Broglie wavelength of the electrons is 0.123 Å. The electrons hit the target at a small angle of 1–8° relative to the surface plane making the formation of a RHEED pattern extremely sensitive to the surface geometry. Nevertheless, the incident electron beam penetrates slightly into the crystal and hence, a RHEED pattern includes also some signal from the (1×1) bulk planes. The diffraction is described by the Laue condition as for LEED. In addition to the change in the electron momentum perpendicular to a surface, the diffraction process leads to a change of the momentum parallel to the surface. This gives rise to a set of diffracted beams on either side of the specular reflected beam. If the incident electron beam is parallel to the rows of surface atoms that are separated by the lattice vector d_S in the direction perpendicular to the beam direction, then the diffracted electron beams contribute to constructive interference. The angle of diffracted electrons relative to the incident direction, θ, fulfills the well-known formula: $d_S \sin \theta = n\lambda_E$, where n is an integer.

For fabrication of high-quality semiconductor devices, it is of utmost importance to start with a substrate having a surface which is structurally well-defined (with a good crystal structure) and is free from amorphous oxides and carbon contaminants. LEED and RHEED are very useful tools for checking whether the substrate surface is clean and well ordered. Nevertheless, it is well known that a substrate surface exhibiting reasonable LEED and RHEED patterns could still have contaminated areas with poor crystalline quality. This is because the LEED and RHEED electrons have a short coherence length, and hence the diameter of the maximum surface area from which emitted electrons add coherently to the intensity is about 10–50 nm for LEED and 50–100 nm for RHEED. Based on this estimation, we could also say that RHEED is somewhat more sensitive to surface defects than LEED. The coherence length of electrons should not be mixed with macroscopic probe areas of electron beams which are of an order of a millimeter in diameter. We should note here that X-ray photoelectron spectroscopy (XPS) and scanning tunneling microscopy (STM) are routinely used to provide complementary information on the surface quality. Although LEED and RHEED do not provide chemical information about surfaces, they are faster to use than, for example STM and XPS, for assessing the surface quality. The absence of the diffraction spots indicates that a surface layer is amorphous (e.g., badly oxidized). If the bulk-plane related (1×1) pattern appears with a strong background intensity, the surface must be cleaned to obtain sharp spots with a low background intensity. Furthermore, clean and well-defined semiconductor surfaces are usually reconstructed. Thus, the LEED or RHEED pattern from such a well-ordered substrate surface should include extra "superstructure" intensity spots in addition to the (1×1) spots. In RHEED, narrow and intensive streaks indicate a smooth surface. It is still worth noting that monitoring LEED or RHEED during the surface cleaning is also helpful to determine the integer (1×1) spots (or streaks) for the pattern analysis described below.

In terms of application, RHEED has certain advantages over LEED: it provides an opportunity for real-time in-situ monitoring of the surface structure during a layer growth, and can be used to determine the growth rate of epitaxial layers. We should mention that LEED can also be utilized in real-time in-situ manner for studying the surface under a heat treatment and/or short time exposure to an adsorbate flux. LEED observations have been increasingly performed also at low temperatures, however one should be aware of possible electron beam-induced changes in surface structures at temperatures below 40 K [13]. The normal features of RHEED and LEED are summarized in Table 1.1.

## 1.2   Analysis of LEED and RHEED Patterns

The left column of Fig. 1.2 illustrates the real space lattice cells for an unreconstructed cubic bulk (100) plane and some of the reconstructed surfaces whose *superlattices* are simply related to the $(100)(1 \times 1)$ plane structure. The right column of Fig. 1.2 illustrates the corresponding LEED patterns that visualize the

Table 1.1 Comparison of the normal features of RHEED and LEED

	RHEED	LEED
Electron energy	5–50 keV	10–500 eV
Electron beam diameter	~1 mm	~1 mm
Coherence length	50–100 nm	10–50 nm
Electron incidence angle	1–8° from surface plane	About perpendicular to surface
Vacuum condition	$<10^{-3}$ mbar	$<10^{-7}$ mbar
Applicable to monitor epitaxy in situ	Yes; MBE chamber is usually equipped with RHEED	No
Use	To monitor epitaxy, to determine surface lattice, to elucidate surface atomic structures by comparing measured and calculated diffraction intensity curves	To determine surface lattice, to elucidate surface atomic structures by comparing measured and calculated diffraction intensity curves
Strength	Easy and quick probe of surface lattice, can be employed in situ in MBE, enables atomic structure determination even with accuracy of 1/100 of atom radius	Easy and quick probe of the surface lattice from a single pattern, different ordered reconstructions coexisting on the surface can be readily concluded, enables atomic structure determination even with accuracy of 1/100 of atom radius
Weakness	Does not give a 2D picture of lattice, solution of the atomic structure requires extensive calculations	Not sensitive to local surface defects, solution of the atomic structure requires extensive calculations

reciprocal lattices. On the basis of such information about the reciprocal lattices, one can determine the lattice vectors and cell of the surface studied by LEED, which further is essential to solving a structural unit cell of the surface (e.g., those in Figs. 1.3 and 1.4). The relative change in the reciprocal-lattice vector length (and cell area) for a surface layer, as illustrated by LEED, is inversely proportional to the corresponding change in the surface lattice dimensions, as compared to the bulk plane. The surfaces are often expressed in terms of the Wood notation [2–5]: $S(hkl)(n \times m)R\theta - A$, where $S(hkl)$ gives the crystal plane of the material with the chemical composition of S, n and m are the proportional lengths of the vectors defining the real-space surface lattice compared to the reference vectors of the (1×1) bulk plane, θ is the angle of possible rotation between the lattices contributing to the reconstruction, and A is the possible adsorbate that induces the reconstruction. The $R\theta - A$ term is not marked if the rotation angle is zero and the surface layer consists of only the substrate elements. The surface lattice may partially match with the bulk plane lattice; in this case, the surface layer is called *commensurate*. If the surface lattice does not match with the bulk structure at all, the surface is termed *incommensurate*. An *incommensurate* structure may form, for example, on adsorbate-covered surfaces in which the adsorbate layer is weakly

Fig. 1.2 Schematic lattices (*left column*) and reciprocal lattices (*right column*), as visualized by LEED, with cells for a cubic (100)(1 × 1) bulk-plane terminated surface and the reconstructed (100)(2 × 1), −(1 × 2), and −c(4 × 4) surfaces. The *black dots* describe the bulk-plane lattice [or represent the integer (1 × 1) LEED spots], and *open circles* describe the surface lattice (or represent the additional reconstruction-related LEED spots)
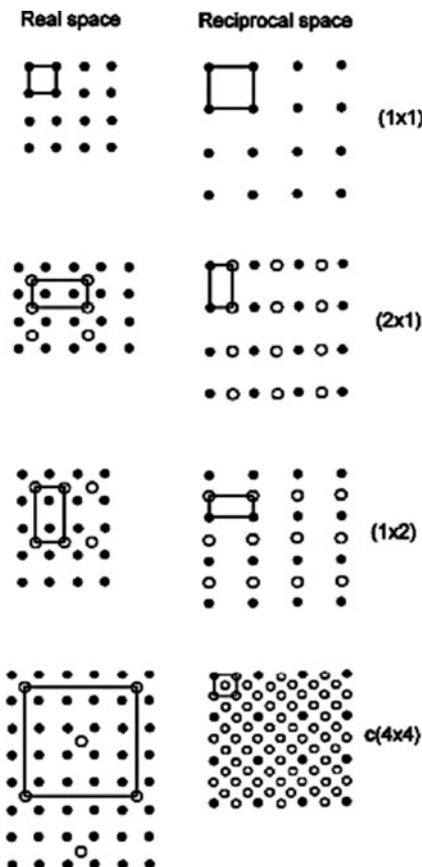
bonded to a substrate. The Wood's notation is not always applicable, and a matrix notation must be used for the surface lattice description [2–5]. The letter "c" is used in front of the Wood $(n \times m)$ term if the surface has a centered lattice cell. A further note is that it is possible to describe a surface with different cells; equally well, a III–V(100)c(4 × 4) surface (Fig. 1.2) may be described with a primitive $(2\sqrt{2} \times 2\sqrt{2})R45°$ cell of which area is smaller than the c(4 × 4) area.

Figure 1.3 shows examples of RHEED and LEED patterns corresponding to (2 × 1)-reconstructed and bulk-terminated (1 × 1) surfaces of a III–V(100) substrate. It also shows possible atomic structures causing the patterns. It can be observed as an essential difference between LEED and RHEED: a single LEED pattern visualizes the two-dimensional reciprocal lattice, while a RHEED pattern gives the reciprocal lattice periodicity only in one crystal direction. Therefore, in order to study the lattice periodicity in the orthogonal direction using RHEED, the sample must be rotated by 90°. This particular feature of RHEED makes it sometimes difficult to decide whether there are two or more surface reconstructions coexisting on a substrate. The RHEED pattern shown in Fig. 1.3 illustrates the reciprocal lattice

Fig. 1.3 RHEED and LEED examples for III–V(100)(1 × 1) and −(2 × 1) surfaces, with possible atomic arrangements. The reciprocal lattice of an unreconstructed III–V(100)(1 × 1) surface is identical to that of the bulk plane. The vectors, defined by the (00) and (10) spots and the (00) and (01) spots, represent the reciprocal lattice vectors for the bulk plane, as visualized by LEED. For a reconstructed III–V(100)(2 × 1) surface, the two vectors defined by the (00) and (1/2 0) spots and the (00) and (01) spots determine the reciprocal lattice of a surface layer. The *gray square* and *rectangle* represent the surface lattice cells
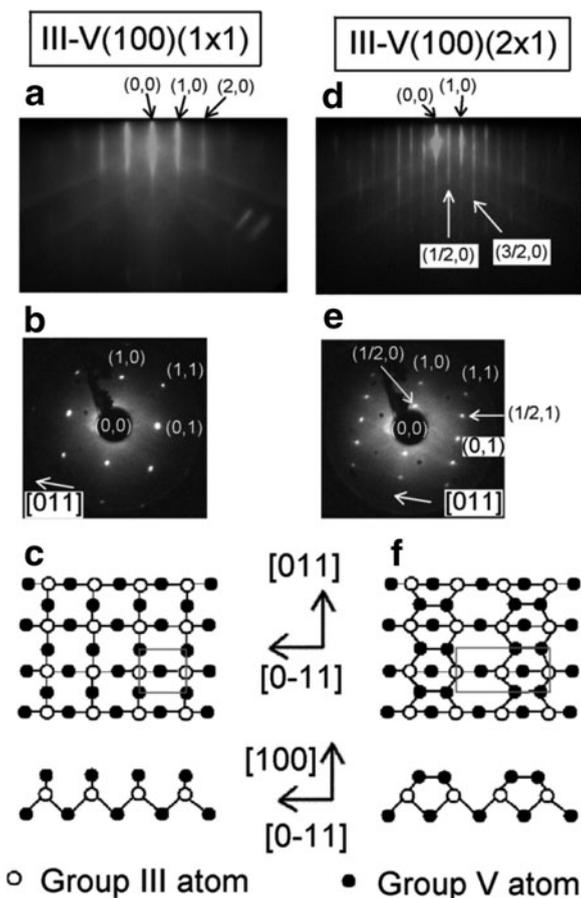
in the [0-11] direction, while the electron beam lies in the [011] direction. If the electron beam lies in the [0-11] direction, then RHEED patterns from the (1 × 1) and (2 × 1) surfaces resemble that of Fig. 1.3a. For the (2 × 1)-reconstructed surface, both the RHEED and LEED patterns reveal the 1/2 fraction spots (or streaks) between the integer (1 × 1) spots; that is, the length of the reciprocal lattice vector of a surface layer, defined by the (00) and (1/2 0) spots, is half of the length of the reciprocal vector for the bulk plane in the [0-11] direction. This means doubling of the lattice cell length for the surface layer in the same [0-11] direction, as compared to the bulk (1 × 1) lattice. It should be noted that for the square and rectangle lattices, the directions of the lattice vectors are identical to the corresponding reciprocal vector directions [2–5]. In the case of III–V(100) surfaces, the doubling usually means that surface atoms form new bonds creating new pairs, so-called dimers. All the surface layers considered in this chapter are simply related to the bulk plane lattices (i.e., are the *superstructures*).
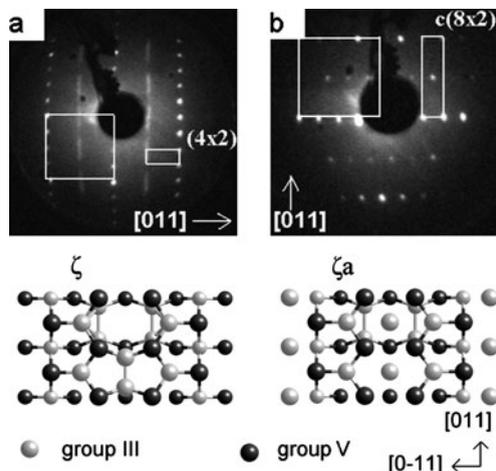
Fig. 1.4 The LEED patterns from (**a**) InAs(100)(4×2) and (**b**) InSb(100)c(8×2) substrate surfaces (please see the text also). The electron energies were (**a**) 55 eV and (**b**) 44 eV. The reciprocal cell of the bulk plane is illustrated by the *white square* and the surface cell by the *white rectangle*. The InAs and InSb substrate pieces were rotated in the different positions relative to the LEED equipment. Two most likely (4×2) structural unit cells, which describe both the InAs(100)(4 × 2) and InSb(100)c(8 × 2) surfaces, are also shown

1.3　Using LEED to Study III–V Surfaces

1.3.1　The c(8 × 2) Surfaces of InAs(100) and InSb(100)

Figure 1.4 shows typical LEED patterns from InAs(100) and InSb(100) surfaces. The substrate surfaces were cleaned by argon-ion sputtering (1.5 keV, 10 mA, for 0.5 h) heating the substrate at a temperature of about 300°C and by subsequent heating for 0.5 h to 470 and 440°C, respectively. This cycle was repeated six times before the patterns shown in Fig. 1.4 were observed. The surface cleanness was confirmed by STM and XPS measurements.

For the interpretation of LEED patterns, it is helpful to determine the integer intensity spots (00), (10), (01), and (11) that set and visualize the reciprocal lattice vectors and cell for a bulk plane, i.e., the reference (1 × 1) reciprocal cell. Often the intensity of the integer spots is higher than that of other possible spots, because the integer spots include also the signal from the bulk planes, and does not depend on the electron energy as strongly as the intensity of the additional spots. The cubic zinc-blende III–V(100) substrates, predominantly used for fabrication optoelectronics devices, have the square lattice as well as reciprocal lattice for the bulk plane as shown in Fig. 1.2. The square areas indicated in Fig. 1.4 represent the reciprocal cells for the InAs(100) and InSb(100) planes. The side lengths of these squares can be readily determined with the (1 × 1) spots along the [011] direction.

Fig. 1.5 (**a**) The III–V(100)(1 × 1) and — (4 × 2) real-space lattice cells. (**b**) The arrangement of the (4 × 2) cells that would cause a clear (4 × 2) LEED pattern. (**c**) The (4 × 2)-cell arrangement for the InSb(100)c(8 × 2) LEED in Fig. 1.4. (**d**) A possible (4 × 2)-cell arrangement which causes the ×2 streaks instead of the ×2 spots in the LEED pattern of the InAs(100)(4 × 2) in Fig. 1.4
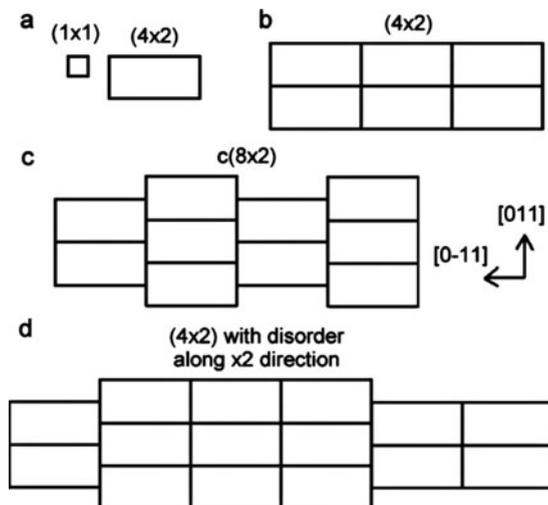
The other, fraction LEED spots in Fig. 1.4, evidence the reconstruction and the change in the reciprocal lattice (and further in the lattice) of a surface layer for both the InAs(100) and InSb(100) substrates. The reciprocal cells for these InAs(100)(4× 2) and InSb(100)c(8 × 2) surfaces are shown in Fig. 1.4. Two most-likely structural unit cells for the reconstructions are also shown in Fig. 1.4 indicating a significant rearrangement of the surface atoms. These atomic models were solved by combining STM, diffraction measurements, and ab initio calculations [14–17]. The (4 × 2) lattice cell arrangement that causes the c(8 × 2) periodicity is illustrated in Fig. 1.5; both surfaces can be described by the (4 × 2) cells shown in Fig. 1.4. It appears that the ×2 order is more visible on the InSb surface than on the InAs surface (Fig. 1.4); this can be linked to some stacking disorder in the ×2 lattice direction on the InAs(100)(4 × 2) surface. On the basis of the shown LEED pattern, it is not clear whether the InAs(100) surface layer has the (4×2) or c(8×2) lattice. A possible reason for the lattice disorder is schematically shown in Fig. 1.5. We also note that the In-V(100)c(8 × 2)/(4 × 2) surface is potentially useful as a starting substrate for producing high-quality III–V heterointerfaces [18] and insulator—III–V interfaces [19, 20]. These types of insulator interfaces are required for the development of future metal-oxide-semiconductor field effect transistors (MOSFETs) with reduced power consumption and prolonged lifetime.

1.3.2 The GaAs(100) Reconstructions

The GaAs(100) is one of the most studied semiconductor surfaces [21–40]. LEED patterns from the common GaAs(100) reconstructions are shown in Fig. 1.6. The reconstructions depend on the substrate treatment and are often related to the amount of arsenic on the surface and the substrate temperature. For example, the
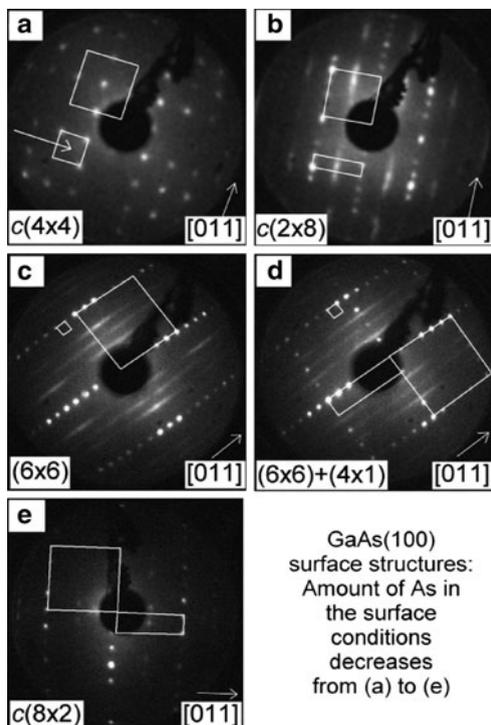
Fig. 1.6 LEED from the GaAs(100) surface reconstructions with decreasing the As amount in the surface conditions from (**a**) to (**e**). The *white squares* represent the (1×1) bulk-plane reciprocal cells and the *white rectangles* represent the reciprocal lattice cells of the surface layers. In pattern (**a**), the *smaller white square* is the c(4×4) cell, in which the *white arrow* shows the missing spot of the c(4×4). This spot was seen with different electron energies. The $6 \times$ streaks in (**c**) and (**d**) arise most likely from the same type of the disorder as described for the InAs(100)(4×2) in Fig. 1.5. In pattern (**d**), the (4×1) cell is drawn instead of the (4×2) because the $\times 2$ streak or spots were not seen properly. In contrast, in the pattern (**e**) those $\times 2$ spots are clearly seen

GaAs(100)c(4×4) surface, of which LEED is shown in Fig. 1.6a, was obtained by heating an arsenic-capped GaAs(100) substrate in UHV overnight at 320°C. The As-cap layer was deposited by MBE onto a 100-nm GaAs buffer layer that was grown on n-type GaAs(100). We should note that it is not easy to determine the absolute temperature of a sample accurately; the errors may be as large as ±25°C, partly due to variations of the temperature across the substrate. Anyway, an increase of the substrate temperature to 530°C changed the GaAs(100)c(4×4) surface to the GaAs(100)c(2×8) or $-(2 \times 4)$ one (Fig. 1.6b). The most likely atomic structures of the III-As(100)c(2×8) or (2×4) surfaces, which often appear during the epitaxial growth of III-As alloys, are the β2 and α2 [26, 32, 34, 38, 39]. When the GaAs(100) substrate is further heated to 580°C, a (6×6) LEED pattern appears as shown in Fig. 1.6c. Prolonged heating leads to the coexistence of two different lattices: (6×6) and $4 \times$ spots as reveled in Fig. 1.6d. Sometimes, this phenomenon complicates

the interpretation of LEED patterns. STM graphs confirmed the presence of areas exhibiting the (6×6) reconstruction as well as of areas with the 4× row structure. We note here that the areas with a ×2 order might be too small to produce the (4 × 2) or c(8 × 2) LEED periodicity in Fig. 1.6d. Further heating did not yield the pure (4 × 2) or c(8 × 2) pattern; this might be due to the presence of residual arsenic in the chamber and partial adsorption of arsenic back to the GaAs surface during its cooling. In a separate experiment, the sputtering cleaning and subsequent heating to 580°C resulted in a pure c(8 × 2) pattern as shown in Fig. 1.6e. The c(8 × 2) pattern corresponds to the atomic structure labeled ξ in Fig. 1.4 [14]. According to ab initio calculations [40], the GaAs(100)(6 × 6) surface is energetically unstable and represents an exceptional case since all the other phases, i.e., c(4 × 4), (2 × 4), and c(8 × 2) are stable.

The information gained by analyzing the series of patterns (LEED or RHEED) can be used to identify the crystal orientations. For example, one might not readily conclude whether a pattern is (2 × 4) or (4 × 2) when measuring a substrate piece cut from the full wafer, but the surface directions can be unambiguously determined by monitoring the change of the patterns. For the InAs(100), the reconstructions follow a change from c(4 × 4) to (2 × 4)/c(2 × 8) and then c(8 × 2) when decreasing the amount of As on the surface [28, 31, 33, 41–46]. For the InSb(100), the pattern changes from (4 × 4) through c(2 × 6) and (1 × 3) to c(8 × 2) when the Sb content on the surface decreases [46–50]. The GaSb(100) exhibits c(2 × 10), c(2 × 6), and (1 × 3) reconstructions [50–55] while the InP(100) surfaces are characterized by the c(4 × 4) and (2 × 4) reconstructions [56–64]. Thus, the GaSb(100) and InP(100) do not show the intrinsic c(8 × 2) and (4 × 2) patterns. It is worth noticing that the InP(100) produces the (2 × 4) pattern for a large range of the surface conditions, making a RHEED optimization of the InP growth with this reconstruction difficult. The occurrence of the c(8 × 2) pattern for the InP(100) substrate usually indicates that a thin InAs(100) layer has been formed during arsenic exposure.

1.3.3 The Bi-Induced Reconstructions on III–V(100)

Understanding the Bi-induced surface reconstructions is essential for advancing the epitaxy of relatively unexplored III–V–Bi compounds and the Bi-surfactant-mediated epitaxy. This section is focused on discussing the Bi-induced reconstructions observed so far.

As a surfactant, Bi floats on the growth front with little incorporation into the crystal. The Bi surfactant has been reported to smoothen the growth of an III–V overlayer [65–69] and to improve the photoluminescence (PL) of dilute nitride GaInAsN quantum wells (QWs) [66]. It also enhances nitrogen incorporation into GaAsN [68,70] and removes a CuPt-like order of GaInP layers [71,72]. Sometimes, it is hard to detect the presence of Bi on a substrate surface by LEED or RHEED because Bi induces the reconstructions quite similar to those induced by the other group-V elements. Nevertheless, there are "fingerprint patterns" associated with

Bi. Such an example is a Bi-induced (1×3) on the GaAs(100) [65–67]. This reconstruction can be observed, for example, when depositing Bi by MBE onto the GaAs(100)(2×4) substrate while keeping the arsenic valve closed and decreasing the substrate temperature. When further decreasing the substrate temperature after observing the (1×3) pattern, the GaAs(100)c(4×4)-Bi surface is formed under a Bi flux. Another "fingerprint" of Bi is an appearance of a (2×1) pattern [67, 73]. This GaAs(100)(2×1)-Bi reconstruction is unusual due to its metallic character [73, 74] and might improve the atomic diffusion on the growth front [73]. The (2×1) pattern corresponds to the less As-rich surface [73,74] in contrast to the GaAs(100)(1×3)-Bi surface which is more As rich. Apparently, there is no report so far in the literature concerning the structural study of the GaAs(100)(1×3)-Bi.

Other fingerprint reconstructions induced by Bi include a (2×8) phase on the InAs and InP(100) substrates, a c(2×10) pattern on the InSb(100) substrate, and a very interesting c(2×12) structure on the InAs(100) surface. For the latter, the LEED pattern indicates the dimer-row separation in the [011] direction to be $6 \times a_{(1 \times 1)}$, where $a_{(1 \times 1)} = 4.3$ Å is the length of the (1×1) square lattice of the InAs(100) bulk plane. On the other hand, STM reveals that the dimer row separation is $10 \times a_{(1 \times 1)}$ and that twisting of the dimer rows leads to a c(2×12) pattern [75]. Indeed, it was observed that the heating of the c(2×12) surface straightened the dimer rows and led to a (2×10) pattern. This large lattice cell causes a very dense row of the LEED spots and complicates the determination of the spot separation.

The Bi-induced reconstructions found so far can be summarized as follows. The addition of Bi on the GaAs(100)c(8×2) surface and the subsequent heating induce the (2×4) pattern, if the maximum Bi coverage is 0.5 ML, and the (2×1) pattern for the Bi coverage between 0.5 and 1.0 ML. If the substrate has the GaAs(100)(2×4) or $-$c(4×4) starting surface, Bi induces the (1×3) pattern, which changes to the c(4×4) one at lower temperatures. Bismuth desorbs strongly from the GaAs(100) at about 450°C. The corresponding desorption temperature for the InAs(100) is about 350°C. When starting with the InAs(100)c(8×2) surface, Bi produces (2×4), (2×8), and (2×1) patterns, for up to 1 ML coverage, and further the (2×10) and c(2×12) reconstructions for a coverage of 1–1.5 MLs. Except for the c(2×12) and (2×10), the same series of reconstructions has been observed on the InP(100)(2×4); here, Bi desorbs at about 400°C. When starting with the InSb(100)c(8×2) surface and increasing the Bi coverage to 1 ML, the reconstruction evolves from (1×3) to c(2×6) and finally to (2×5); the strong desorption takes place at about 300°C.

1.4 Using RHEED to Study III–Vs

1.4.1 Optimizing the Growth Conditions of GaAs/AlAs Heterostructures

Although the GaAs/AlAs interfaces have been studied for several decades, it has remained somewhat unclear what it is the optimum As/group-III flux ratio for

the growth of low-dimensional structures, such as multiquantum wells (MQWs). This issue was recently addressed by combining RHEED observations and photoluminescence measurements for GaAs/AlAs MQWs [76]. The results show that an optimum flux ratio is near the conditions corresponding to a change in the GaAs(100) reconstruction from (2 × 4) to (4 × 2). The main findings of this study are presented in Fig. 1.7 and serve as an example of how RHEED can be utilized to control and understand the epitaxial growth. The RHEED patterns were obtained during the growth of the GaAs and AlAs layers at different substrate temperatures while decreasing the As flux. The (2 × 4) pattern changed first to a (1 × 1) and then to (4 × 2). The growth time in the (1 × 1) and (4 × 2) conditions was minimized because they are known to result in poor quality of the crystal.

1.4.2 The GaAs(100) Reconstructions

Figure 1.8 shows the RHEED patterns for three different reconstructions on the GaAs(100) substrate. The more intense streaks of the GaAs(100)(4 × 6) are the integer diffractions, and their distance provides the reference reciprocal vector length of the bulk plane while the less intense streaks are the fraction diffractions. The streaky and sharp patterns indicate smooth GaAs(100) surfaces. The (4 × 6) and (2 × 4) patterns were obtained at the substrate temperature of about 550°C, i.e.,
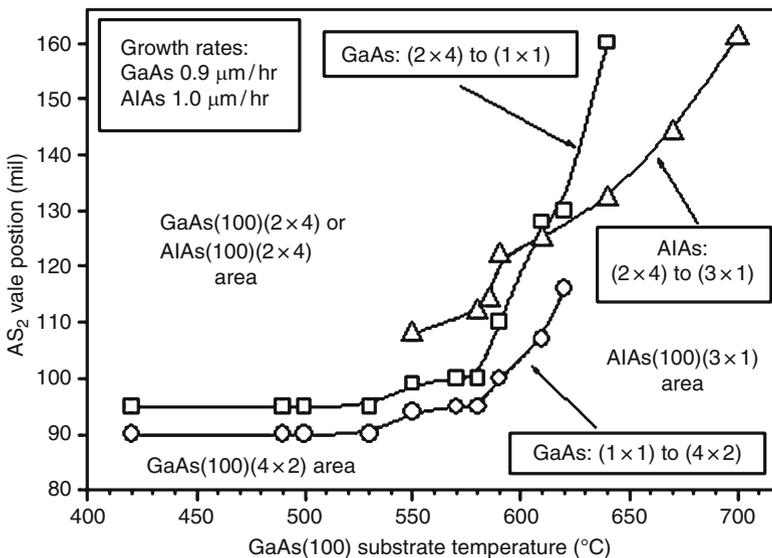

Fig. 1.7 A diagram showing how the GaAs(100) and AlAs(100) surface structures change by tuning the substrate temperature and As flux during the epitaxial growth. The 100-mil As flux corresponds to the As/Ga flux ratio of 5 and to the As/Al flux ratio of 18 approximately

Fig. 1.8 RHEED patterns for different GaAs(100) reconstructions in different surface directions. The more intense streaks of the GaAs(100)(4 × 6) are the integer diffractions and visualize the (1 × 1) reciprocal cell side while the less intense streaks are the fraction diffractions. For the GaAs(100)c(4 × 4), it is also shown the diffraction along the [010] direction, i.e., the 45° rotation relative to the [011]. Its integer streak distance is smaller than that along the [011] or [0-11] direction and is divided in the four equal parts (some of the fraction streaks are weaker than the other ones), please see also Fig. 1.2
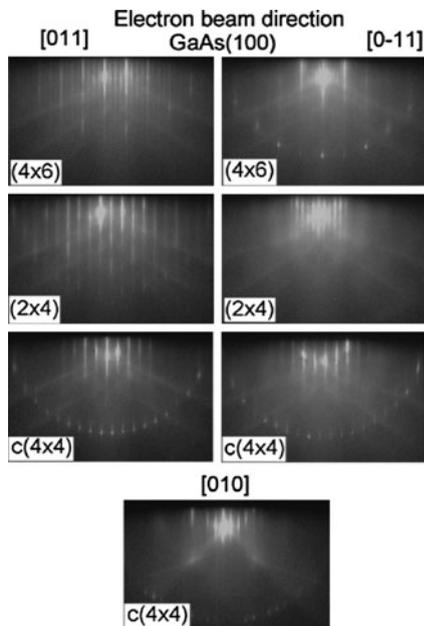
30°C higher than the temperature at which the transition from (2 × 4) to c(4 × 4) occurs under the 1×10^{-7} mbar As flux. The (4 × 6) pattern was obtained by closing the As shutter and exposing the surface to Ga flux. Most likely, this RHEED pattern corresponds to a Ga-rich surface as reported recently [37], but it cannot be excluded from the possibility that the surface included both the (4 × 1) and (6 × 6) areas, as shown by the LEED images of Fig. 1.6d. The c(4 × 4) pattern was observed at the substrate temperature of 480°C for an As_2 flux corresponding to a partial pressure of 1×10^{-7} mbar. This c(4 × 4) reconstruction remained stable after the As flux was closed and the substrate temperature was decreased.

1.4.3 The GaAs(111) Reconstructions

The GaAs(111)A substrate surface exhibits only (2 × 2) reconstruction while GaAs(111)B surface reveals also a more complicated ($\sqrt{19} \times \sqrt{19}$)$R23.4°$ reconstruction [77–81]. The (2 × 2) and ($\sqrt{19} \times \sqrt{19}$)$R23.4°$ patterns were found on the GaAs(111)B substrate at the temperatures of 480 and 520°C, respectively and an As pressure of about 1×10^{-7} mbar. The GaAs(111)A surface exhibits a (2 × 2) pattern for a wide range of the surface conditions. For example, for the same As pressure of about 1×10^{-7} mbar, the (2 × 2) RHEED pattern is maintained for substrate temperatures ranging from 350 to 590°C, and it does not change visually at all. Therefore, it might be difficult to optimize the growth parameters of these surfaces

using with the (2×2) RHEED. It is worth noting that the $(\sqrt{19} \times \sqrt{19})R23.4°$ reconstruction on the GaAs(111)B surface is an exception because it appears to be a metallic surface with partially filled dangling bonds. The metallic character of the III–V surface might be a useful growth front [82].

### 1.4.4 Probing Surface Reconstructions in GaInAsN(100)

In this section, we discuss the reconstructions of dilute nitride (GaInAsN) lattice matched to the GaAs(100) and having a N content of about 3%. The RHEED patterns were monitored as a function of the substrate temperature and the As flux. For the growth temperatures within 300–400°C, only a (1×3) reconstruction was observed (Fig. 1.9). Heating the GaInAsN film and supplying As flux modified the reconstruction from a c(4×4) pattern at temperatures below 300°C to the (1×3) pattern for temperatures within 300–450°C. Further change to a (2×4) pattern occurred for a temperature range of 500–570°C. Closing the As flux at 570°C produced a (3×1) pattern. The GaInAsN(100)(1×3) reconstruction is interesting because usually it is not seen on the III-As(100) surfaces. The observation agrees with recent calculations proving that the (4×3) reconstructions are almost stable on the GaAs(100) and are likely important in kinetically limited growth conditions as well as for strain-stabilized III–V alloy surfaces [83]. Thus the (1×3) RHEED observation provides an experimental evidence for the calculated results; the surfaces producing a (1×3) pattern are, in fact, composed of (4×3) building blocks [50, 55]. We would like to remind the reader that depending on the measurement by which the lattice periodicity has been determined (e.g., RHEED or STM), the same surface may be called (1×3) or c(2×6). Actually, more recent measurements and calculations have revealed that the real unit cell is (4×3) and not (1×3), although it is sometimes referred as the (1×3) reconstruction. The (1×3), c(2×6), and (4×3) reconstructions are similar to each other because these surfaces consist of dimer rows with the $\times 3$ separation.

The (3×1) reconstruction found on the GaInAsN(100) in less As-rich conditions is also rather exceptional; to our knowledge it appears only on the AlAs(100) in the less As-rich concentrations, as shown in the diagram of Fig. 1.7. LEED and XPS experiments showed that the heating of the GaInAsN in UHV yielded a (3×1) surface structure and concomitantly led to indium segregation toward the surface.

1.4.5 In-Situ Calibrations of Growth Rate and Composition of Multinary Compounds

RHEED has been instrumental for the development of MBE technology and is nowadays a standard part of MBE growth chambers. Besides its use for obtaining real-time information on the growth modes and surface morphology, it provides

Fig. 1.9 RHEED patterns of
GaInAsN films (N content
around 3%) lattice matched to
the GaAs(100) substrate
during growth stops under the
As flux in two perpendicular
directions
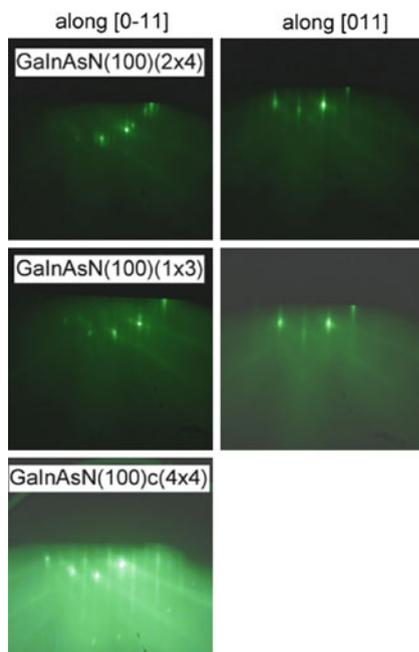
also an easy way to calibrate the growth rates of binary alloys with atomic layer
precision [84]. The growth rate can be determined by measuring the time required
to complete the deposition of an atomic layer. This is done by monitoring the
intensity variation of the specular RHEED spot, which depends on the surface
roughness: the maximum intensity is obtained when an atomic layer is completed,
while a minimum is obtained for an incomplete layer with a maximum disorder [a
growth front is still reconstructed during the growth, e.g., the (2×4)-reconstructed
GaAs]. The intensity oscillations are analyzed with an image processing software,
which plots the oscillation as a function of time. An example of such intensity
oscillations is shown in Fig. 1.10. In order to avoid errors due to the fluctuations
of the growth conditions, the growth rate is determined by measuring the time
required to complete several oscillations. The procedure is repeated several times by
closing and opening the shutter controlling the flux of the material that determines
the growth rate (e.g., Ga in the case of GaAs).

The variation of RHEED intensity oscillations and their amplitude damping
behavior could reveal other important aspects regarding the growth kinetics [84, 85]
and can be used for the composition calibration of ternary (or multinary) alloys,
as discussed next. Usually, the MBE growth is performed in excess flux of one of
the components (e.g., As in the case of arsenides and Ga in the case of GaN). When
growing a ternary compound, i.e., adding a third element, the growth rate of the layer
increases proportionally to the additional flux. Knowing the sticking coefficient for
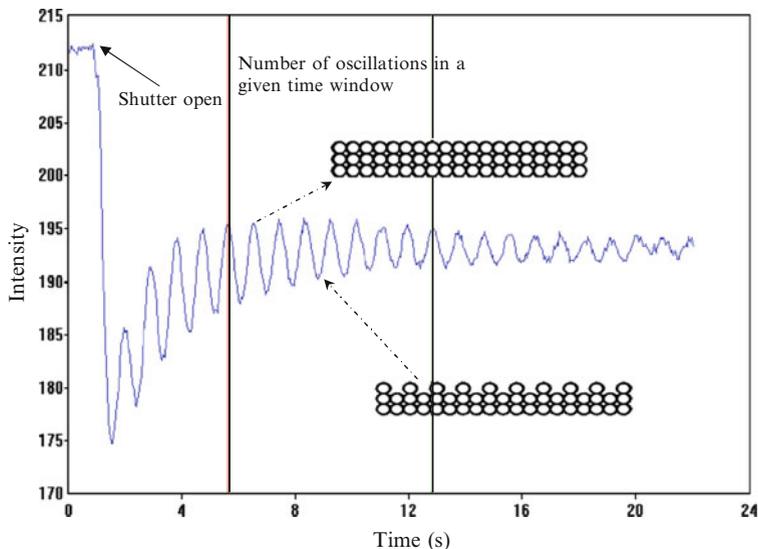the given flux (usually equal to one for the III elements in the MBE growth), one

Fig. 1.10 An example of possible intensity oscillation of the specular RHEED beam from a GaAs(100) surface. The period corresponds to the growth rate of a GaAs monolayer

may calibrate the composition of the ternary compound in a simple way. Next we show how this method can be applied for calibrating the growth rate of InGaAs and GaSbAs ternary alloys.

In the case of the $In_x Ga_{1-x}As$, by measuring the growth rates of GaAs, r_{GaAs}, and InGaAs, r_{InGaAs}, we can determine the In content (x), as being equal to $x = (r_{InGaAs} - r_{GaAs})/r_{InGaAs}$. For a concrete example, Fig. 1.11 shows the oscillation of the RHEED specular spot during deposition of GaAs and subsequent deposition of InGaAs. The growth was performed on the GaAs(100) using the substrate temperature of 480°C. The oscillations have been recorded with the RHEED beam parallel to the [010] azimuth. The estimated composition of In was ~14%.

We should note that applicability of this method for composition evaluation is dependent on the lattice mismatch between the compound grown for the calibration purposes (InGaAs in this case) and the substrate/buffer layer. For example, it is not possible to grow several ML-thick InAs binary alloy on GaAs(100) because the critical thickness for growing two-dimensional layer-by-layer InAs is below two MLs. For an InGaAs ternary alloy, the critical thickness for growth on the GaAs(100) substrate depends on the In content; for the In content exceeding 30%, it drops below 7 nm rendering difficult the use of RHEED for composition calibration. In this case, higher Ga flux is used to test the InGaAs growth rate and In composition while for the final target structure, the Ga flux is decreased. In the case of quaternary alloy, such as $Al_x In_y Ga_{1-x-y}As$, the Al contents (x) and In contents (y) can be estimated by measuring the growth rates of AlAs, GaAs, and InGaAs and r_{GaAs}, r_{InGaAs}, and r_{AlAs}, respectively. Then the composition of

Fig. 1.11 RHEED intensity oscillations (specular spot in the [010] azimuth) recorded for GaAs (*upper panel*) and subsequently grown InGaAs (*lower panel*). The In contents calculated from the increase of the InGaAs growth rate with respect to GaAs is equal to 14%
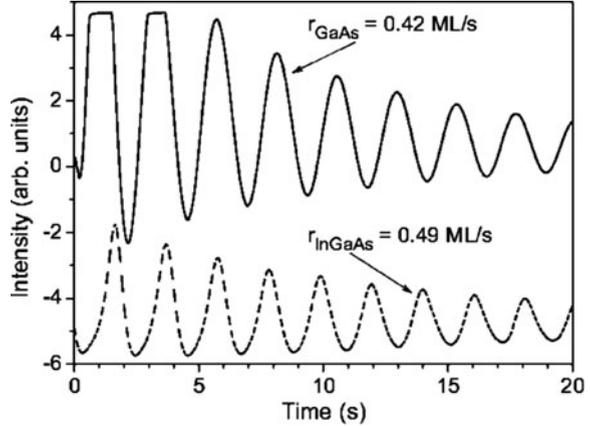
the quaternary alloy can be estimated as being $x = r_{AlAs}/(r_{InGaAs} + r_{AlAs})$ and $y = (r_{InGaAs} - r_{GaAs})/(r_{InGaAs} + r_{AlAs})$.

The applicability of this method is limited to the multinary alloys with the intermixed III elements (e.g., InGaAs and AlGaAs). For alloys with the mixed V elements, like GaAsSb, GaAsP, and GaAsN, the use of this method is much more difficult, or sometimes impossible, because the growth rates are limited by the elements of the group III (i.e., they do not depend on the group V fluxes). In some special cases, this problem can be overcome. For example, reducing the group-V flux and depositing 2–3 MLs of the III element (Ga in the case of GaAs), one gets a group III-rich surface (e.g., Ga). Exposing this Ga-rich surface to the flux of V element will result in 2–3 RHEED intensity oscillations. Then the growth rate determined from the period of these oscillations is proportional to the impinging V element flux.

1.5 Concluding Remarks

Crystalline interfaces and thin films are the building blocks of many advanced semiconductor devices as well as devices not existing currently. Any improvement in the ordering at the junction will decrease the defect density, having clear implications on the device lifetime and energy consumption. These well-defined materials also make it possible to elucidate their fundamental atomic and electronic structures with detailed measurements and calculations. The engineering of the well-defined growth fronts has a key role in the manufacturing of crystalline interfaces and films. This chapter introduced the LEED and RHEED methods which are routinely used by crystal growers to monitor the surfaces of crystalline films. The LEED and RHEED patterns visualize the reciprocal lattice of the surface layer studied, from which the surface lattice can be readily constructed. The examples

discussed dealt with the III–V semiconductor surfaces, which exhibit various reconstructions as a function of the substrate temperature and III/V atom ratio. The literature abounds in many results showing how the starting surface reconstructions are linked to the quality of the III–V interfaces and grown films. Here we have presented a series of diffraction patterns for a few technologically important III–V(100) substrate surfaces. Knowing the type of reconstruction required one could identify adequate growth conditions for the fabrication of novel crystalline films and related device structures.

References

1. J. Mannhart et al., Science **327**, 1607 (2010)
2. A. Zangwill, *Physics at Surfaces* (Cambridge University Press, Cambridge, 1988)
3. W.N. Unertl (ed.), in *Physical Structure. Handbook of Surface Science*, vol. 1, (Elsevier Science B.V., The Netherlands, 1996)
4. H. Lüth, *Solid Surfaces, Interfaces and Thin Films* (Springer, New York, 2001)
5. F. Bechstedt, *Principles of Surface Physics* (Springer, New York, 2003)
6. P.K. Larsen, P.J. Dobson (eds), *Reflection High-Energy Electron Diffraction and Reflection Electron Imaging of Surfaces* (Plenum, New York, 1988)
7. K. Heinz, Progr. Surf. Sci. **27**, 239 (1988)
8. J.B. Pendry, Surf. Sci. Rep. **19**, 87 (1993)
9. Q.-K. Xue, T. Hashizume, T. Sakurai, Progr. Surf. Sci. **56**, 1 (1997)
10. A. Ohtake, Surf. Sci. Rep. **63**, 295 (2008)
11. C. Davisson, L.H. Germer, Nature **119**, 558 (1927)
12. C. Davisson, L.H. Germer, Phys. Rev. **30**, 705 (1927)
13. T. Uda, H. Shigekawa, Y. Sugawara, S. Mizuno, H. Tochihara, Y. Yamashita, J. Yoshinobu, K. Nakatsuji, H. Kawai, F. Komori, Progr. Surf. Sci. **76**, 147 (2004)
14. S.-H. Lee, W. Moritz, M. Scheffler, Phys. Rev. Lett. **85**, 3890 (2000)
15. C. Kumpf, L.D. Marks, D. Ellis, D. Smilgies, E. Landemark, M. Nielsen, R. Feidenhans'l, J. Zegenhagen, O. Bunk, J.H. Zeysing, Y. Su, R.L. Johnson, Phys. Rev. Lett. **86**, 3586 (2001)
16. C. Kumpf, D. Smilgies, E. Landemark, M. Nielsen, R. Feidenhans'l, O. Bunk, J.H. Zeysing, Y. Su, R.L. Johnson, L. Cao, J. Zegenhagen, B.O. Fimland, L.D. Marks, D. Ellis, Phys. Rev. B **64**, 075307 (2001)
17. J.J.K. Lång, M.P.J. Punkkinen, P. Laukkanen, M. Kuzmin, V. Tuominen, M. Pessa, M. Guina, I.J. Väyrynen, K. Kokko, B. Johansson, L. Vitos, Phys. Rev. B **81**, 245305 (2010)
18. T. Anan, S. Sugou, K. Nishi, Appl. Phys. Lett. **63**, 1047 (1993)
19. H.-S. Kim, I. Ok, M. Zhang, F. Zhu, S. Park, J. Yum, H. Zhao, J.C. Lee, P. Majhi, N. Goel, W. Tsai, C.K. Gaspe, M.B. Santos, Appl. Phys. Lett. **93**, 062111 (2008)
20. B. Shin, D. Choi, J.S. Harris, P.C. McIntyre, Appl. Phys. Lett. **93**, 052911 (2008)

21. M.D. Pashley, K.W. Haberern, W. Friday, J.M. Woodall, P.D. Kirchner, Phys. Rev. Lett. **60**, 2176 (1988)
22. D.K. Biegelsen, R.D. Bringans, J.E. Northrup, L.-E. Swartz, Phys. Rev. B **41**, 5701 (1990)
23. S.L. Skala, J.S. Hubacek, J.R. Tucker, J.W. Lyding, S.T. Chou, K.-Y. Cheng, Phys. Rev. B **48**, 9138 (1993)
24. C.W. Snyder, J. Sudijono, C.-H. Lam, M.D. Johnson, B.G. Orr, Phys. Rev. B **50**, 18194 (1994)
25. J.E. Northrup, S. Froyen, Phys. Rev. B **50**, R2015 (1994)
26. T. Hashizume, Q.-K. Xue, J. Zhou, A. Ichimiya, T. Sakurai, Phys. Rev. Lett. **73**, 2208 (1995)
27. T. Hashizume, Q.-K. Xue, A. Ichimiya, T. Sakurai, Phys. Rev. B **51**, 4200 (1995)
28. H. Yamaguchi, Y. Horikoshi, Phys. Rev. B **51**, 9836 (1995)
29. W.G. Schmidt, F. Bechstedt, Phys. Rev. B **54**, 16742 (1996)
30. Y. Garreau, M. Sauvage-Simkin, N. Jedrecy, R. Pinchaux, M.B. Veron, Phys. Rev. B **54**, 17638 (1996)
31. Q.-K. Xue, T. Hashizume, T. Sakurai, Prog. Surf. Sci. **56**, 1 (1997)
32. V.P. LaBella, H. Yang, D.W. Bullock, P.M. Thibado, P. Kratzer, M. Scheffler, Phys. Rev. Lett. **83**, 2989 (1999)
33. G.R. Bell, J.G. Belk, C.F. McConville, T.S. Jones, Phys. Rev. B **59**, 2947 (1999)
34. W.G. Schmidt, S. Mirbt, F. Bechstedt, Phys. Rev. B **62**, 8087 (2000)
35. A. Ohtake, J. Nakamura, S. Tsukamoto, N. Koguchi, A. Natori, Phys. Rev. Lett. **89**, 206102 (2002)
36. A. Ohtake, N. Koguchi, Appl. Phys. Lett. **83**, 5193 (2003)
37. A. Ohtake, P. Kocán, K. Seino, W.G. Schmidt, N. Koguchi, Phys. Rev. Lett. **93**, 266101 (2004)
38. P. Laukkanen, M. Kuzmin, R.E. Perälä, M. Ahola, S. Mattila, I.J. Väyrynen, J. Sadowski, J. Konttinen, T. Jouhti, C.S. Peng, M. Saarinen, M. Pessa, Phys. Rev. B **72**, 045321 (2005)
39. A. Ohtake, Phys. Rev. B **74**, 165322 (2006)
40. K. Seino, W.G. Schmidt, A. Ohtake, Phys. Rev. B **73**, 035317 (2006)
41. C. Kendrick, G. LeLay, A. Kahn, Phys. Rev. B **54**, 17877 (1996)
42. M. Göthelid, Y. Garreau, M. Sauvage-Simkin, R. Pinchaux, A. Cricenti, G. Le Lay, Phys. Rev. B **59**, 15285 (1999)
43. C. Ratsch, W. Barvosa-Carter, F. Grosse, J.H.G. Owen, J.J. Zinck, Phys. Rev. B **62**, R7719 (2000)
44. R.H. Miwa, G.P. Srivastava, Phys. Rev. B **62**, 15778 (2000)
45. F. Grosse, W. Barvosa-Carter, J.J. Zinck, M.F. Gyure, Phys. Rev. B **66**, 75321 (2002)
46. P. Laukkanen, M.P.J. Punkkinen, M. Ahola-Tuomi, J. Lång, M. Kuzmin, J. Sadowski, J. Adell, R.E. Perälä, M. Ropo, K. Kokko, L. Vitos, B. Johansson, M. Pessa, I.J. Väyrynen, J. Electron. Spectros. Relat. Phenom. **177**, 52 (2010)
47. A.G. de Oliveira, S.D. Parker, R. Droopad, B.A. Joyce, Surf. Sci. **227**, 150 (1990)
48. C.F. McConville, T.S. Jones, F.M. Leibsle, S.M. Driver, T.C.Q. Noakes, M.O. Schweitzer, N.V. Richardson, Phys. Rev. B **50**, 14965 (1994)
49. P.R. Varekamp, M.C. Håkansson, J. Kanski, D.K. Shuh, M. Björkqvist, M. Gothelid, W.C. Simpson, U.O. Karlsson, J.A. Yarmoff, Phys. Rev. B **54**, 2101 (1996)
50. P. Laukkanen, M.P.J. Punkkinen, N. Räsänen, M. Ahola-Tuomi, J. Sadowski, J. Adell, M. Kuzmin, J. Lång, R.E. Perälä, M. Ropo, K. Kokko, L. Vitos, B. Johansson, M. Pessa, I.J. Väyrynen, Phys. Rev. B **81**, 035310 (2010)
51. G.E. Franklin, D.H. Rich, A. Samsavar, E.S. Hirschorn, F.M. Leibsle, T. Miller, T.-C. Chiang, Phys. Rev. B **41**, 12619 (1990)
52. M.T. Sieger, T. Miller, T.-C. Chiang, Phys. Rev. B **52**, 8256 (1995)
53. J. Olde, K.-M. Behrens, H.-P. Barnscheidt, R. Manzke, M. Skibowski, J. Henk, W. Schattke, Phys. Rev. B **44**, 6312 (1991)
54. U. Resch-Esser, N. Esser, B. Brar, H. Kroemer, Phys. Rev. B **55**, 15401 (1997)
55. W. Barvosa-Carter, A.S. Bracker, J.C. Culbertson, B.Z. Nosho, B.V. Shanabrook, L.J. Whitman, H. Kim, N.A. Modine, E. Kaxiras, Phys. Rev. Lett. **84**, 4649 (2000)
56. V.P. LaBella, Z. Ding, D.W. Bullock, C. Emery, P.M. Thibado, J. Vac. Sci. Tech. A **18**, 1492 (2000)

57. C.D. MacPherson, R.A. Wolkow, C.E.J. Mitchell, A.B. McLean, Phys. Rev. Lett. **77**, 691 (1996)
58. W.G. Schmidt, F. Bechstedt, N. Esser, M. Pristovsek, Ch. Schultz, W. Richter, Phys. Rev. B **57**, 14596 (1998)
59. W.G. Schmidt, F. Bechstedt, Surf. Sci. **409**, 474 (1998)
60. S. Mirbt, N. Moll, K. Cho, J.D. Joannopoulos, Phys. Rev. B **60**, 13283 (1999)
61. N. Esser, W.G. Schmidt, J. Bernholc, A.M. Frisch, P. Vogt, M. Zorn, M. Pristovsek, W. Richter, F. Bechstedt, Th. Hannappel, S. Visbeck, J. Vac. Sci. Tech. B **17**, 1691 (1999)
62. L. Li, Q. Fu, C.H. Li, B.-K. Han, R.F. Hicks, Phys. Rev. B **61**, 10223 (2000)
63. K. Lüdge, P. Vogt, O. Pulci, N. Esser, F. Bechstedt, W. Richter, Phys. Rev. B **62**, R11046 (2000)
64. P. Vogt, K. Ludge, M. Zorn, M. Pristovsek, W. Braun, W. Richter, N. Esser, Phys. Rev. B **62**, R12601 (2000)
65. M.R. Pillai, S.-S. Kim, S.T. Ho, S.A. Barnett, J. Vac. Sci. Tech. B **18**, 1232 (2000)
66. S. Tixier, M. Adamcyk, E.C. Young, J.H. Schmid, T. Tiedje, J. Cryst. Growth **251**, 449 (2003)
67. G. Feng, K. Oe, M. Yoshimoto, J. Cryst. Growth **301–302**, 121 (2007)
68. T. Liu S. Chandril, A.J. Ptak, D. Korakakis, T.H. Myers, J. Cryst. Growth **304**, 402 (2007)
69. A.J. Ptak, R. France, C.-S. Jiang, R.C. Reedy, J. Vac. Sci. Tech. B **26**, 1053 (2008)
70. E.C. Young, S. Tixier, T. Tiedje, J. Cryst. Growth **279**, 316 (2005)
71. S.W. Jun, C.M. Fetzer, R.T. Lee, J.K. Shurtleff, G.B. Stringfellow, Appl. Phys. Lett. **76**, 2716 (2000)
72. S.W. Jun, G.B. Stringfellow, J.K. Shurtleff, R.-T. Lee, J. Cryst. Growth **235**, 15 (2002)
73. M.P.J. Punkkinen, P. Laukkanen, H.-P. Komsa, M. Ahola-Tuomi, N. Räsänen, K. Kokko, M. Kuzmin, J. Adell, J. Sadowski, R.E. Perälä, M. Ropo, A. Tukiainen, T.T. Rantala, I.J. Väyrynen, M. Pessa, L. Vitos, J. Kollár, S. Mirbt, B. Johansson, Phys. Rev. B **78**, 195304 (2008)
74. P. Laukkanen, M.P.J. Punkkinen, H.-P. Komsa, M. Ahola-Tuomi, K. Kokko, M. Kuzmin, J. Adell, J. Sadowski, R.E. Perälä, M. Ropo, T.T. Rantala, I.J. Väyrynen, M. Pessa, L. Vitos, J. Kollár, S. Mirbt, B. Johansson, Phys. Rev. Lett. **100**, 086101 (2008)
75. M. Ahola-Tuomi, P. Laukkanen, M.P.J. Punkkinen, R.E. Perälä, I.J. Väyrynen, M. Kuzmin, K. Schulte, M. Pessa, Appl. Phys. Lett. **92**, 011926 (2008)
76. J. Pakarinen, V. Polojärvi, P. Laukkanen, A. Tukiainen, A. Laakso, C.S. Peng, P. Tuomisto, V.-M. Korpijärvi, J. Puustinen, M. Pessa, Appl. Surf. Sci. **255**, 2985 (2008)
77. E. Kaxiras, K.C. Pandey, Y. Bar-Yam, J.D. Joannopoulos, Phys. Rev. Lett. **57**, 923 (1986)
78. K.W. Haberern, M.D. Pashley, Phys. Rev. B **41**, 3226 (1990)
79. J.M.C. Thornton, P. Weightman, D.A. Woolf, C.J. Dunscombe, Phys. Rev. B **51**, 14459 (1995)
80. A. Taguchi, K. Shiraishi, T. Ito, Phys. Rev. B **60**, 11509 (1999)
81. A. Ohtake, J. Nakamura, T. Komura, T. Hanada, T. Yao, H. Kuramochi, M. Ozeki, Phys. Rev. B **64**, 045318 (2001)
82. J. Neugebauer, T.K. Zywietz, M. Scheffler, J.E. Northrup, H. Chen, R.M. Feenstra, Phys. Rev. Lett. **90**, 056101 (2003)
83. J.C. Thomas, N.A. Modine, J. Mirecki Millunchick, A. Van der Ven, Phys. Rev. B **82**, 165434 (2010)
84. J.H. Neave, B.A. Joyce, P.J. Dobson, N. Norton, Appl. Phys. A **81**, 1 (1983)
85. B.A. Joyce, J. Zhang, T. Shitara, J.H. Neave, A. Taylor, S. Armstrong, M.E. Pemble, C.T. Foxon, J. Cryst. Growth **115**, 338 (1991)